Neptunium(V) Coprecipitation with Calcite

ARTICLE *in* ENVIRONMENTAL SCIENCE AND TECHNOLOGY · FEBRUARY 2008

Impact Factor: 5.33 · DOI: 10.1021/es071790g · Source: PubMed

3 AUTHORS, INCLUDING:

Frank Heberling
Karlsruhe Institute of Technology
21 PUBLICATIONS **193** CITATIONS
SEE PROFILE

Melissa Anne Denecke
The University of Manchester
184 PUBLICATIONS **2,700** CITATIONS
SEE PROFILE

Article

Neptunium(V) Coprecipitation with Calcite

Frank Heberling, Melissa A. Denecke, and Dirk Bosbach

Environ. Sci. Technol., **2008**, 42 (2), 471-476• DOI: 10.1021/es071790g • Publication Date (Web): 07 December 2007

Neptunium(V) Coprecipitation with Calcite

FRANK HEBERLING,* MELISSA A. DENECKE, AND DIRK BOSBACH

Institut für Nukleare Entsorgung (INE), Forschungszentrum Karlsruhe, PO Box 3640, 76021 Karlsruhe, Germany

Received July 20, 2007. Revised manuscript received October 09, 2007. Accepted October 25, 2007.

Coprecipitation experiments of Np(V) and U(VI) with calcite were performed in mixed-flow reactors under steady state conditions at room temperature for up to 400 h at precipitation rates of 1.0×10^{-8} to 6.8×10^{-8} mol/(m^2 s). The saturation index with respect to calcite varied between 0.04 and 0.95. Initial Np(V) or U(VI) concentrations were 1 μmol/L, 0.01 mol/L NaCl was used as background electrolyte, and pH ranged from 7.8 to 12.8. Partition coefficients for Np(V) were in the range of 0.5−10.3, compared to 0.02 for U(VI). Np L_{III} and U L_{III} EXAFS were used to characterize the local structural environment of the incorporated actinides. In the case of U(VI), the structural environment is not unambiguously characterized. Our data suggest that Np(V) ions occupy calcium lattice sites. The two axial oxygen atoms of the linear neptunyl moiety substitute two calcite carbonate groups in the first coordination sphere. Thus, four carbonate groups coordinate the neptunyl-ion in a monodentate fashion with four equatorial oxygen atoms (O_{eq}) at 2.4 Å and associated carbon atoms (C) at 3.2 Å. The interatomic distances indicate slight structural relaxation of the carbonate groups from their ideal sites. A similar structural model has been reported for U(VI) incorporated into natural calcite.

Introduction

The disposal of high-level nuclear waste in deep geological formations poses major scientific and social challenges to be met in the next decades. One of the key issues is the long-term safety of a waste repository system over extended periods of time, up to 10^6 years. Demonstrating the repository safety over such geological time spans requires a sound understanding of the geochemical behavior of long-lived and radiotoxic radionuclides such as the actinides (*1*). The actinide elements U, Np, and Pu form oxo-cations ("actinyl-cations") in oxidizing aqueous environments (*2, 3*). The environmental behavior of the actinyl ions $U(VI)O_2^{2+}$, $Np(V)O_2^{+}$, and $Pu(V,VI)O_2^{(+,2+)}$ is, to a large extent, controlled by sorption reactions (inner- and outer-sphere surface complexation, ion-exchange, coprecipitation/structural incorporation) with minerals. Calcite is a common mineral in most rock types which are currently considered for deep geological waste disposal (*4, 5*), and the goal of this study is to elucidate the mechanism of uranyl and neptunyl sorption to calcite.

Molecular level actinyl−calcite interaction in aqueous environments appears to be complex and not unambiguously characterized, as various, sometimes contradictory results have been reported in the literature. A number of studies have characterized the sorption behavior of U(VI) and Np(V) onto calcite by means of macroscopic batch-type experiments (*6–10*). Recently, it was shown that Np(V) sorption is affected by pH and carbonate alkalinity (*9*). Spectroscopic data characterizing the calcite–water interface in the presence of U(VI) (*8, 11, 12*) have been reported. Extended X-ray absorption fine structure (EXAFS) spectroscopy data indicate the formation of an inner-sphere surface complex. Luminescence spectroscopy data suggest the presence of two surface sorbed U(VI) species (*13*): the aqueous U(VI) triscarbonato complex and a second species with a luminescence signal intermediate between that of the aqueous triscarbonato complex and that of U(VI) incorporated into calcite. Polarization dependent grazing incidence (GI)EXAFS measurements suggest that the calcite sorbed U(VI) species is not identical with the aqueous U(VI) triscarbonato complex (*12*). X-ray standing wave (XSW) measurements seem to suggest the formation of monodentate surface complexes preferentially along monomolecular acute steps and terrace planes (*14*).

Coprecipitation of U(VI) with calcite has been studied experimentally in recent years (*15–18*). Uptake of U(VI) during calcite precipitation is rather limited with partition coefficients ranging from ~0.01 to 0.26 (*19*) and a maximal U concentration of 1900 ppm in the precipitate. μ-XRF measurements of synthetic U doped calcite crystals reveal a distinct sector zoning, which indicates that preferential adsorption/incorporation contributes to site-selective U uptake during calcite precipitation (*20*). It also indicates nonequilibrium conditions for such coprecipitated U containing calcite crystals. EXAFS studies on experimentally precipitated U(VI) containing calcite indicate that UO_2^{2+} becomes incorporated. The uranyl ion retains its two axial oxygen (O_{ax}) neighbors but exhibits a carbonate coordination which is different from the Ca^{2+} — CO_3^{2-} coordination in calcite (*15, 16*). In contrast to aqueous carbonato complexes, five equatorial oxygens (O_{eq}) at a distance of 2.33–2.36 Å and a split carbon coordination sphere with carbon atoms at 2.9 and 3.2 Å have been found. This indicates a combination of monodentate and bidentate bound carbonate groups with significant static disorder, as indicated by their Debye–Waller factors (*15, 16*).

Some natural U(VI) containing calcite crystals seem to contain U(VI) in a structural configuration slightly different than the synthetic samples (*21, 22*). For example, Kelly et al. (*22*) found U(VI) in a structural environment in a 298 Ma old natural calcite, which is compatible with a model where U(VI) substitutes for Ca^{2+}. An elongated $U-O_{ax}$ distance of 1.867 Å and about four O_{eq} atoms at a distance of 2.31 Å indicate significant structural relaxation and enhanced compatibility of the incorporated U(VI) species with the calcite structure.

The small partition coefficient as well as the structural distortion caused by U(VI) incorporation into calcite during coprecipitation experiments seem to suggest a significant structural incompatibility. However, the fact that natural calcite crystals contain U(VI) in a comparatively less distorted structural environment may indicate the stability of U(VI) doped crystals under certain geochemical conditions over extended periods of time.

Here, we study the structural incorporation of Np(V) into calcite via coprecipitation under well defined conditions and compare it to the incorporation of U(VI). The aim of this work is to ascertain if neptunyl ions can be incorporated into the calcite crystal structure at stable sites and to quantify

* Corresponding author phone: +49 (0)7247 82-4782; e-mail: Frank.Heberling@ine.fzk.de.

10.1021/es071790g CCC: $40.75
Published on Web 12/07/2007

TABLE 1. Experimental Conditions and Results of the MFR Experiments[a]

	pH_{input} (±0.05)	$c_{in}(Ca^{2+})$ [mmol/L] (±6.6%)	$c_{in}(AnO_2^{+,2+})$ [μmol/L] (±6.6%)	c_{in}(TIC) [mmol/L] (±0.5%)	SI_{input} (±20%)	surface area [m^2] (±9%)	flowrate [mL/min] (±1.5%)
Cc1	10.39	0.28		0.8	1.06	0.205	0.61
Np1	10.38	0.34	0.92	0.8	1.14	0.208	0.52
Np2	10.40	0.35	0.80	0.8	1.16	0.207	0.50
Np3	12.85	1.30	0.87	1.0	1.26	0.205	0.60
Np4	8.22	2.36	1.10	8.0	1.30	0.208	0.53
U1	8.21	2.80	1.01	8.0	1.36	0.205	0.58

	pH_{output} (±0.05)	$c_{out}(Ca^{2+})$ [mmol/L] (±6.6%)	$c_{out}(AnO_2^{+,2+})$ [μmol/L] (±6.6%)	Np/U content [ppm] (±35%)	SI_{output} (±20%)	*R*(calcite) [$\times 10^{-8}$ mol/($m^2 \cdot s$)] (±30%)	*D* (±25%)
Cc1	10.13	0.04			0.04	1.19	
Np1	10.26	0.09	0.14	5249	0.43	1.04	2.0
Np2	10.15	0.07	0.26	3248	0.26	1.13	0.5
Np3	12.77	0.64	0.10	1966	0.57	3.22	7.5
Np4	8.08	1.54	0.17	1912	0.95	3.48	10.3
U1	7.80	1.36	0.99	23	0.59	6.79	0.02

[a] Estimated uncertainties for measured and calculated values are given in column headings in parentheses.

the uptake by the homogeneous Henderson−Kracek partition coefficient (*23*). The structural environment of neptunyl and uranyl coprecipitated with calcite is characterized by EXAFS analysis in order to identify the substitution mechanism.

Experimental Section

Coprecipitation experiments are performed using a mixed-flow-reactor (MFR), which allows coprecipitation of homogeneous Np(V) or U(VI) containing calcite onto calcite seed crystals. In the 45 mL MFR-volume a stirring bar keeps a sieved fraction of calcite powder in suspension. The stirring bar is suspended to avoid grinding effects. The diameter of the calcite seed crystals is chosen between 11 and 15 μm to minimize the boundary layer effect and to ensure surface reaction controlled coprecipitation kinetics (*24, 25*). As seed crystals we use ∼160 mg sieved Merck suprapur calcium carbonate with an XRD powder pattern showing lines uniquely of calcite. The specific surface of the crystal seeds is measured by BET to be 1.28 m^2/g. Thus the initial calcite surface area in the reactor is ∼0.2 m^2 (Table 1), with an uncertainty of 9%.

Three independent solution reservoirs are used to feed the reactor with aqueous Np(V)/U(VI), Ca^{2+}, and HCO_3^-/CO_3^{2-} solutions. The solutions are prepared with MilliQ water (18.2 MΩ·cm) and Merck p.a. chemicals. Composition of the solutions in the different experiments is shown in Table 1. For pH adjustment the carbonate solution is prepared in different ways: pH 8.2 is reached by dissolving 8 mmol/L $NaHCO_3$, pH 10.3 using 0.8 mmol/L Na_2CO_3, and pH 12.8 by dissolving 1 mmol/L Na_2CO_3 in 0.3 mol/L NaOH. Input pH is measured giving an aliquot of each input solution into a sample tube. Input saturation index with respect to calcite, SI_{input}, is calculated with PhreeqC (*26*) and the Nagra/PSI chemical thermodynamic database (*27*) using this pH value and the measured solution concentrations ($SI = \log_{10}(IAP/K_{sp})$, with IAP, the ion activity product, and K_{sp}, the solubility product). There is no gas phase in the MFR. We try to avoid reactions between the solutions and air CO_2 by sealing the solution reservoirs. pH of the carbonate input solution is checked frequently and in case it decreases by more than 0.2 pH units due to the influence of air CO_2 a fresh solution is prepared. For the other solutions reaction with air CO_2 can be neglected.

Six experiments are conducted under different experimental conditions as summarized in Table 1: (Cc1) a pure calcium carbonate system without actinides as reference at pH 10.13; (Np1 and Np2) Np(V) coprecipitation at pH ∼10.2; (Np3) Np(V) coprecipitation at pH 12.77; (Np4) Np(V) coprecipitation at pH 8.08, and (U1) U(VI) coprecipitation at pH 7.8.

Solutions from the three reservoirs are pumped continuously into the MFR by peristaltic pumps for up to 17 days. Calcium and neptunium/uranium concentrations are sampled once before (c_{in}) and daily behind the reactor (c_{out}) and analyzed by means of ICP-MS (Np1−Np4 and U1) or ICP-AES (Cc1). The carbonate concentration of the output solution is not measured directly but estimated assuming that the precipitated amount of carbonate is equal to the amount of precipitated calcium, $c_{out}(TIC) = c_{in}(TIC) - \Delta c(Ca^{2+})$. The flowrate is measured during each sampling procedure. As we assume homogeneous mixing in the MFR, c_{out} and pH_{output} are thought to reflect the steady state conditions within the reactor, where the actinyl containing calcite grows homogeneously onto the seed crystals over a time period, $t_{steady\text{-}state}$. PhreeqC calculations showed that a mixture of the three input solutions as well as the output solution is undersaturated with respect to all solid Np(V) phases for which solubility data are available (*3, 27*). Therefore, the formation of known pure Np(V) phases can be excluded.

From the concentration difference, Δc, ($\Delta c = c_{in} - c_{out}$) the flowrate, and the calcite surface_area we calculate the steady state precipitation rate, *R* (eq 1). We assume that the surface area remains constant within the limit of error (±9%) during the whole experiment.

$$R = \frac{\text{flowrate} \times \Delta c}{\text{surface\_area}} \quad (1)$$

The values for the precipitation rates, *R*, show high uncertainties of about 30%.

We use the homogeneous Henderson–Kracek partition coefficient, *D* (*23*), as a measure for coprecipitation (eq 2):

$$D = \frac{X_{An}/X_{Ca}}{c_{out}(AnO_2^{+/2+})/c_{out}(Ca^{2+})} = \frac{c_{in}(AnO_2^{+/2+})/c_{out}(AnO_2^{+/2+}) - 1}{c_{in}(Ca^{2+})/c_{out}(Ca^{2+}) - 1} \quad (2)$$

Molar fractions X_a of calcium and neptunium or uranium in the precipitate can be calculated as $X_a = \Delta c \times \text{flowrate} \times t_{steady\text{-}state}$. As flowrate and $t_{steady\text{-}state}$ are constant for one experiment, the equation for *D* simplifies as shown in eq 2. Calculated in this manner, the estimated uncertainty of *D* is 25%. Uncertainties are estimated applying standard error-

propagation calculations, with initial errors of 9% for BET surfaces, 6.6% for ICP-MS results, and 1.5% for the flowrates.

After the MFR experiments calcite suspensions are taken out of the reactor volume. The calcite powder sedimentates and is separated from the supernatant. The calcite is filled in PE sample tubes as a wet paste for the EXAFS measurements.

EXAFS measurements are performed at the INE-Beamline for actinide research at ANKA (*28*) in fluorescence-mode using a solid state detector (LEGe Canberra). For measurements at the Np L_{III} edge (17.610 keV) we use Ge(422) as monochromator crystals. Energy calibration is done by parallel measurement of a Zr-foil, defining the first inflection point in the Zr *K*-edge as 17.998 keV. The uranium L_{III}-EXAFS (L_{III} edge at 17.166 keV) is measured using Si(311) crystals, using a Y-foil for energy calibration (Y K-edge, 17.038 keV). Seven to seventeen spectra are averaged and analyzed using backscattering amplitude and phase shift functions calculated with Feff 8 (*29*) and the FEFFIT 2.54 software. Background removal is done with WinXAS 3.1 (*30*). The maximum of the most intense absorption feature, the so-called white line, is set to the ionization energy, E_0, which serves as the origin for generating *k*-values. In the fit procedure E_0 is modified by addition of the relative shift in ionization energy, ΔE_0. The amplitude reduction factor, S_0^2, is adjusted to 0.8 for Np and 0.9 for U, values obtained in preliminary fits assuming that the number of the axial oxygens is two. A S_0^2 of 0.9 for uranium is in good agreement with published theoretical and experimental values (*31, 32*). Fits are performed in *R*-space in the range between 0.7 and 3.5 Å. A Hanning window function is used for the Fourier transformation in a *k*-range of 2.4 to ~12 $Å^{-1}$ for the neptunium spectra and 1.8 to 8.5 $Å^{-1}$ for the uranium spectrum. Only single scattering paths are used to fit the data. The relative shift in ionization energy, ΔE_0, used is 9.2 eV for the neptunium samples and 8.42 eV for the uranium sample.

Results and Discussion

A 0.4−1.5 μm thick homogeneous calcite layer containing 1900–5100 ppm Np(V) has been synthesized onto calcite seed crystals at precipitation rates between 1.04–3.48 × 10^{-8} mol/(m^2·s) (Table 1). An empirical partition coefficient, *D*, (eq 2) is determined to be in the range from 0.5 to 10.3.

The pH has a major effect on the aqueous speciation of Np(V) (*3*). At pH ~10.2 the neptunyl monocarbonato complex dominates (90%) (Np1 + Np2). At pH 12.77 the neptunyl hydroxo and dihydroxo complexes are the major species (18 and 70%, respectively) (Np3). At pH 8.08 the neptunyl monocarbonato complex still dominates the aqueous speciation (76%) but the free NpO_2^+-ion makes about 24% of the Np content (Np4). However, there appears to be no clear correlation between *D* and pH (Table 1). If one substitutes the aqueous concentration ratio cNp(V)/cCa(II) by the activity ratio $\{NpO_2^+\}/\{Ca^{2+}\}$, *D* values would then range from 5 (Np2) to 306 (Np3). This large range is not a consequence of the neptunyl content of the precipitates. Rather it originates from the low NpO_2^+ activity at high pH where carbonato- and hydroxo-complexes dominate the speciation, and free NpO_2^+ is hardly present. Therefore, we conclude that NpO_2^+ incorporation into calcite does not depend on the relative concentration of the NpO_2^+-aqueous species present in the experimental solution. The saturation state of the aqueous solution at which precipitation takes place is expressed as the output saturation index, SI_{output}. SI_{output} lies between 0.04 and 0.95 during the experiments. Under these conditions, supersaturated solutions remain metastable, and no homogeneous nucleation occurs within the time frame of the experiments (*33*).

The coprecipitation rates with Np(V) are generally positively correlated with SI and vary between 1.04 and 3.48 × 10^{-8} mol/(m^2·s). These rates are small compared to previously published coprecipitation experiments (*19*). The presence of Np(V) in solution reduces the precipitation rate. This effect can be recognized for experiments Cc1 and Np1/Np2. These experiments are all at comparable pH ~ 10.2 and have reaction rates, which are the same to within the uncertainty ($R \approx 1.1 \times 10^{-8}$ mol/(m^2·s)). However, in experiment Cc1 this reaction rate results from a significantly lower supersaturation level of calcite ($SI_{steady\_state} = SI_{output} = 0.04$) than in the presence of NpO_2^+ in experiments Np1/Np2 (SI_{output} = 0.43, 0.26, respectively). Such crystal growth inhibition effects are known for species in solution which block active crystal growth surface sites (e.g., kink sites) (*34*).

In order to be able to compare our Np(V) coprecipitation experiments to previously published U(VI) coprecipitation experiments, we perform an experiment with U(VI), U1, and one at similar conditions with Np(V), Np4 (SI_{input} 1.3 and pH_{input} 8.2). PhreeqC calculations show that there are no supersaturated uranyl phases at these conditions. From this experiment we derive a *D* of 0.02, corresponding to a 23 ppm U containing calcite (Table 1). This value agrees well with previously published data (*15, 19*). In comparison, the value for *D* in experiment Np4 is 2 orders of magnitude higher than for U1. This indicates Np(V) has a higher affinity for calcite than U(VI). The differences between the Np(V) and U(VI) coprecipitation behavior could be related to the high stability of U(VI) carbonato solution complexes. Under the conditions of experiment U1 the uranyl tris-, and biscarbonato complexes dominate the aquatic uranyl speciation (77 and 23%) (ternary $Ca_{1,2}UO_2(CO_3)_3^{2-,0}$ complexes have not been considered in the speciation calculation), whereas the monocarbonato complex and the free neptunyl ion dominate the Np(V) speciation (76 and 24%) in Np4. Assuming that this difference in solution speciation originates from a higher affinity of uranyl for bidentate complexation by carbonate ions offers a plausible explanation for the lower compatibility/affinity of the uranyl cation to the calcite structure.

The crystal growth inhibition effect observed for Np(V) is less effective for U(VI) (Table 1). The conditions in experiments Np4 and U1 are very similar, but the precipitation rate in the presence of U(VI) is twice as high as in the presence of Np(V). This lower crystal growth inhibition effect as well as the lower partition coefficient of U(VI) reflects its weaker interaction with calcite compared to Np(V).

It is important to emphasize that the *D* values derived from our experiments describe the composition of a mixed phase precipitated from a supersaturated solution of a defined composition. As mentioned above, previous site specific incorporation studies indicate that incorporation of foreign ions into calcite depends on crystal morphology indicating nonequilibrium conditions (sector and intrasectoral zoning) (*20, 35*).

The k^2-weighted EXAFS spectra (small diagrams) and their Fourier transform (FT) spectra in *R*-space are shown in figure 1 together with the corresponding model (fit result) spectra. Spectra in *R*-space are not corrected for phase shift. Structural parameters obtained from the EXAFS analyses are summarized in Table 2. The distance from the central Np atom to the axial oxygens (O_{ax}) is 1.86 ± 0.01 Å. In the equatorial plane the neptunyl ion is coordinated by about four oxygen atoms (O_{eq}) at 2.40 ± 0.01 Å distance. The coordination numbers for the more distant scattering paths (C/O_2) are also about four for Np1 and Np2. The coordination numbers for these paths for samples Np3 and Np4 did not yield a stable fit so they are held constant at four during the fit procedure without any significant increase in the highly correlated Debye–Waller factor values. Measured Np−C distances range from 3.10 to 3.21 Å, R(Np−O_2) from 3.35 to 3.45 Å.

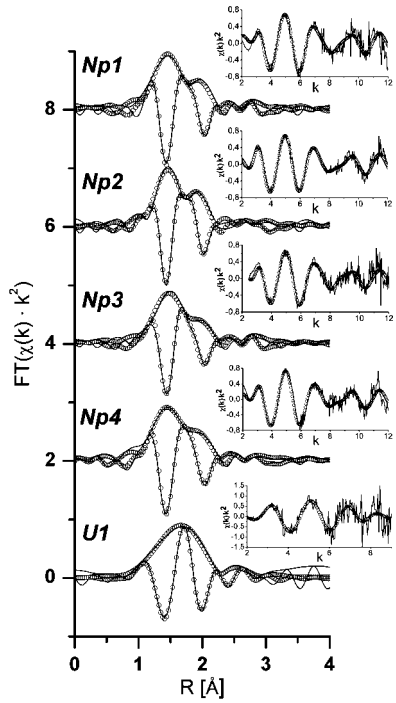

FIGURE 1. Fourier transform amplitude and imaginary part of the k^2-weighted EXAFS data (lines) and model spectra (circles). Spectra are not corrected for phase shift and they are offset along the ordinate for clarity. The original EXAFS data in *k*-space together with the corresponding fits are shown in the small diagrams above each Fourier transformed spectrum.

In order to interpret these EXAFS analysis results, let us turn to the coordination structure of known Np(V) compounds. Pentavalent neptunium forms a linear NpO_2^+ complex in aqueous environments. Np−O_{ax} distances range from 1.82 to 1.90 Å in solid neptunyl phases with equatorial oxygen coordination (*36*). Atoms comprising the equatorial plane coordination show much stronger interatomic distance variability. Solid Np(V)-phases are known with four-, five-, and 6-fold equatorial coordination in square, pentagonal, and hexagonal bipyramidal geometry (*36*). In the case of oxygen as nearest neighbor in the equatorial plane, distances are near 2.39 Å for 4-fold coordination, 2.39−2.52 Å for 5-fold coordination, and 2.42−2.64 Å for 6-fold coordination (*36*).

In the aqueous triscarbonato complex ($NpO_2(CO_3)_3^{5-}$) three carbonate ions coordinate Np(V) through bidentate bonds with a Np−O_{eq} distance of 2.53 Å (*37*). Due to the bidentate bonding of the carbonate groups, the Np−C distances are short (2.93−2.98 Å) (*37*). In solid neptunium monocarbonate phases $MNpO_2CO_3$ ($M = Li^+$, Na^+, K^+, NH_4^+, Rb^+, or Cs^+), the neptunyl ion is coordinated by six O_{eq} originating from either three bidentate or two mono and two bidentate carbonate groups, forming hexagonal or orthorhombic (NpO_2CO_3) layers depending on the size of the interlayer cation (*38*).

If we compare these coordination structures to our EXAFS results, we find good agreement between $R(O_{ax}) = 1.86$ Å and that for the solid Np(V) phases described above (1.82−1.90 Å). In contrast to the previously mentioned known structures with 6-fold equatorial coordination, we find an O_{eq} coordination number of about four. Coordination numbers are, however, associated with high uncertainties (Table 2). It is known from bond-valence theory that bond length and coordination number are correlated (*39*), so that bond lengths can serve as a measure for coordination number. The Np−O_{eq} bond length is found to be 2.4 Å. This is in agreement with distances for four-, or 5-fold NpO_2^+ coordination.

TABLE 2. Results of the EXAFS analysis for coordination numbers, *N*, interatomic distances, *R*, and Debye–Waller factors, σ^{2a}

Np1	*N*	*R* [Å]	σ^2 [Å²]
O_{ax}	2.1 (0.4)	1.86 (0.01)	0.0006 (0.0001)
O_{eq}	3.9 (0.9)	2.40 (0.02)	0.0063 (0.0015)
C	4.9 (3.4)	3.1 (0.1)	0.011 (0.008)
O_2	4.3 (2.9)	3.4 (0.1)	0.014 (0.009)
Np2	***N***	***R* [Å]**	**σ^2 [Å²]**
O_{ax}	1.8(0.3)	1.85(0.01)	0.0005(0.0001)
O_{eq}	4.4(0.8)	2.40(0.02)	0.0061(0.0011)
C	3.0(2.9)	3.2(0.1)	0.016(0.015)
O_2	3.8(2.5)	3.4(0.1)	0.015(0.010)
Np3	***N***	***R* [Å]**	**σ^2 [Å²]**
O_{ax}	2.0(0.3)	1.86(0.01)	0.0010[b]
O_{eq}	4.0(0.8)	2.40(0.02)	0.0078(0.0016)
C	4[b]	3.1(0.1)	0.010[b]
O_2	4[b]	3.4(0.1)	0.010[c]
Np4	***N***	***R* [Å]**	**σ^2 [Å²]**
O_{ax}	2.1(0.3)	1.86(0.01)	0.0011(0.0002)
O_{eq}	4.1(0.7)	2.41(0.02)	0.0059(0.0010)
C	4[b]	3.2(0.1)	0.014[b]
O_2	4[b]	3.4(0.1)	0.014[c]
U1	***N***	***R* [Å]**	**σ^2 [Å²]**
O_{ax}	1.7(1.3)	1.83(0.02)	0.0066(0.0050)
O_{eq}	5.6(1.2)	2.38(0.01)	0.0050[b]
C_{bi}	1.9(1.0)	2.9(0.1)	0.0031(0.0016)
C_{mono}	1.9(1.2)	3.3(0.1)	0.0031[c]

[a] Uncertainties (in parentheses) are standard deviations given by the Feffit software. The uncertainties of the coordination numbers are increased about 10% to account for the uncertainty in S_0^2. [b] Held constant during the fit, [c] Correlated to the value of the previous scattering path.

The bond lengths associated with bidentate aqueous neptunyl−carbonato complexes (Np−O_{eq} 2.48−2.53 Å, Np−C distance 2.93−2.98 Å) have a longer Np−O distance and a shorter Np−C distance than the corresponding bond lengths obtained from analysis of our calcite samples (Np−O_{eq} distance 2.4 Å, Np−C 3.1−3.2 Å), This difference can only be explained as monodentate bonding of the coordinating carbonate groups to the central neptunyl ion in our samples. The equal coordination numbers for O_{eq} and carbon (C) are also indication of monodentate carbonate complexation; a bidentate coordination would necessarily cause a N(O_{eq})/N(C) increase.

In the calcite crystal structure, Ca^{2+} ions are coordinated by six monodentate bound carbonate ions. The interatomic distances are Ca−O_1, 2.35 Å, Ca−C, 3.20 Å, and Ca−O_2, 3.44 Å (*40*). If we hypothesize that neptunyl occupies a calcium site in the calcite structure with only four monodentate bound carbonate ions in the first equatorial coordination sphere, the resulting two vacant carbonate sites could leave space for the axial neptunyl oxygen atoms. The Np−O_{eq} distance (2.4 Å) is significantly longer than the Ca−O_1 distance in the calcite structure, but typical for 4-fold equatorial oxygen coordination around neptunyl (*36*). Np−C and Np−O_2 distances are within the limits of error the same as Ca−C and Ca−O_2 distances in the calcite structure. These observations imply that the calcite lattice structure slightly relaxes to fulfill the bond length requirements of the neptunyl ion. The relaxation of the calcite structure by neptunyl incorporation suggests a positive enthalpy of mixing. Therefore,

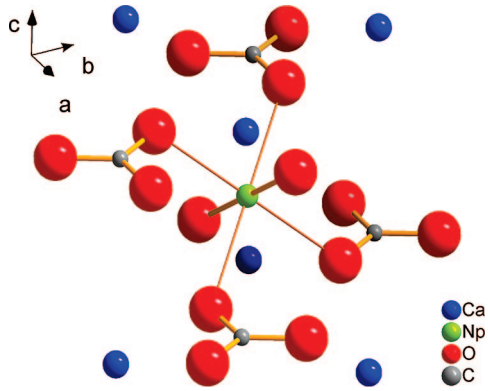

FIGURE 2. Structural model of a neptunyl-ion incorporated into the calcite host. Neptunium(V) is located on a Ca^{2+} site and the two axial neptunyl oxygens substitute for two adjacent carbonate ions. The resulting four monodentate bound carbonate ions and six coordinating Ca^{2+} ions are shown. The coordinate system indicates a possible orientation of this structure relative to the hexagonal calcite lattice.

in a solid-solution series between a neptunyl−carbonate phase and calcite only limited miscibility can be expected, in particular at room temperature. The low Debye–Waller factors obtained from the EXAFS analysis for the O_{ax} and O_{eq} scattering paths indicate a high structural order in the coordination polyhedron of the Np atoms. We interpret the increased Debye–Waller factors (0.010−0.016 Å^2), together with the relatively high uncertainties in bond lengths and coordination numbers for the C and O_2 scattering paths, as indication of disorder in the orientation of the carbonate ions coordinated around the neptunyl ions. That we find solely monodentate carbonate complexation around the neptunyl ion is a strong argument for the structural incorporation of the neptunyl ions into the calcite structure during the coprecipitation experiments. The small disorder introduced into the calcite structure by incorporation of neptunyl suggests a high stability of this structure. A picture of a neptunyl ion incorporated into the calcite structure according to our results is shown in figure 2.

The two missing carbonate ions and the substitution of Ca^{2+} by NpO_2^+ leave a charge excess of +3 in the calcite structure upon neptunyl incorporation. We do not yet have evidence how this charge is balanced. Possible charge balancing mechanisms could be a coupled substitution of Ca^{2+} ions by Na^+ or creation of vacant Ca^{2+} sites. Site-selective time-resolved laser fluorescence investigations of the charge balancing mechanism in Eu(III) containing calcite show strong evidence for the coupled substitution of Na^+ and Eu^{3+} for 2 Ca^{2+} (*41*). An analogous charge balancing mechanism with coupled substitution of Na^+ and NpO_2^+ for Ca^{2+} might also apply here. The critical EXAFS scattering path yielding information about such a coupled substitution mechanism would be the calcium shell surrounding the incorporated neptunyl. However, the distance to the Ca coordination sphere at 4.03 Å (*40*) is too long to be identified from room temperature EXAFS data. Attempts to fit this shell resulted in unreasonably high Debye–Waller factors.

Due to the low uranyl content of sample U1 of about 23 ppm, the usable *k*-range of the EXAFS spectra of this sample is limited (1.8−8.5 Å^{-1}). Data and model curves in *k*- and *R*-space are shown in Figure 1. The EXAFS analysis yields the following results: two O_{ax} at 1.83 Å, five to six (5.6 ± 1.2) O_{eq} at a distance of 2.38 Å from the central U atom. This distance corresponds well with the equatorial bond lengths of U(VI) phases exhibiting 5-fold O_{eq} coordination, 2.37 ± 0.09 Å (*36*). For the carbon coordination sphere the best fit result is obtained if we split the carbon scattering path into two subshells, resulting in carbon atoms at 2.87 Å (C_{bi}) and at 3.33 Å (C_{mono}) (Table 2). This result could be explained by mixed bidentate and monodentate coordination of the carbonate ions around the uranyl in the equatorial plane. Coordination numbers obtained for the C_{bi} and C_{mono} scattering path (1.9 ± 1.0 and 1.9 ± 1.2) make it impossible to differentiate if there is one bidentate and three monodentate bound carbonate ions or two bidentate and only one monodentate bound carbonate in the equatorial plane around the uranyl ion. We tend to interpret this as an indication that there is likely a mixture of the two configurations. Reeder et al. 2000 and 2001 (*15, 16*) find a very similar uranyl environment in synthesized uranyl doped calcite. They report that the uranyl ion is coordinated by five equatorial oxygens originating from three or four carbonate ions, two or one of them bound in bidentate fashion. The bond length to the closest equatorial oxygens O_{eq}, 2.33 Å, is remarkably short in their case. The simultaneous presence of bidentate and monodentate bound carbonate ions suggests that upon coprecipitation uranyl is incorporated into a strongly distorted site, which is not compatible to the calcite structure.

Kelly et al. 2003 and 2006 (*21, 22*) report that uranyl can occupy a stable lattice position in natural calcite samples. From their investigation of U(VI) containing natural calcite samples of different age (13.7 ka and 298 Ma), they suggest that the uranyl environment in calcite might evolve and become more calcite compatible over long time scales. The structure they suggest for the uranyl environment in the younger calcite is very similar to the neptunyl environment in our coprecipitated calcite. If indeed the structural environment of uranyl incorporated into calcite becomes more calcite compatible over geological time spans, whereas neptunyl is incorporated into such a stable site immediately upon coprecipitation, then this is another argument for the higher compatibility of neptunyl and calcite compared to uranyl and calcite. It is, however, difficult to draw conclusions from the comparison of natural and synthesized Np and U doped calcite, as the conditions during formation (e.g., supersaturation, temperature, and uranyl activity) and during geologic periods of time (e.g., diagenesis, heat, and pressure) are usually not precisely known for natural samples.

The experimental results clearly show that neptunyl has a higher affinity for calcite than uranyl. EXAFS analyses revealed equatorial coordination by four monodentate bound carbonate ions for calcite incorporated neptunyl ions. This suggests that neptunyl is structurally incorporated into the calcite host upon coprecipitation and that neptunyl substitutes one Ca^{2+} and two carbonate ions in the calcite structure. Incorporation of NpO_2^+ into a relatively stable site upon coprecipitation indicates the relevance of calcite for long-term retention of neptunium(V) in the geosphere.

Acknowledgments

We thank Boris Brendebach, Kathy Dardenne, and Jörg Rothe of the INE-Beamline for support in EXAFS measurements and in data analysis. Many thanks to Stephanie Heck for her help in the laboratory and to Christian Marquardt for the neptunium supply and support in handling radioactive material. Financial support by the European integrated project FUNMIG is gratefully acknowledged.

Literature Cited

(1) Magill, J.; Berthou, V.; Haas, D.; Galy, J.; Schenkel, R.; Wiese, H. W.; Heusener, G.; Tommasi, J.; Youinou, G. Impact limits of partitioning and transmutation scenarios on the radiotoxicity of actinides in radioactive waste. *Nucl. Energy (Br. Nucl. Energy Soc.* **2003**, *42* (5), 263.

(2) Grenthe, I.; Fuger, J.; Konings, R. J. M.; Lemire, R. J.; Muller, A. B.; Ngyun-Trung Cregu, C.; Wanner, H. *Chemical Thermodynamics of Uranium*; North-Holland: Amsterdam, 1992; Vol. *1*, p 715.

(3) Lemire, R. J.; Fuger, J.; Nitsche, H.; Potter, P.; Rand, M. H.; Rydberg, J.; Spahiu, K.; Sullivan, J. C.; Ullman, W. J.; Vitorge, P.; Wanner, H., *Chemical Thermodynamics of Neptunium and Plutonium*; Elsevier: Amsterdam, 2001; Vol. 4.
(4) NAGRA *Project Opaliunus Clay - Safety Report - Demonstration of Disposal Feasability for Spent Fuel, Vitrified High-Level Waste and Long-Lived Intermediate Waste (Entsorgungsnachweis)*; NAGRA: Wettingen/Switzerland, 2002.
(5) Claret, F.; Sakharov, B. A.; Drits, V. A.; Velde, B.; Meunier, A.; Griffault, L.; Lanson, B. Clay minerals in the Meuse-Haute marne underground laboratory (France): Possible influence of organic matter on clay mineral evolution. *Clay Clay Miner.* **2004**, *52* (5), 515.
(6) Carroll, S. A.; Bruno, J. Mineral-solution iInteractions in the U(VI)-CO_2-H_2O System. *Radiochim. Acta* **1991**, *52–3*, 187.
(7) Carroll, S. A.; Bruno, J.; Petit, J. C.; Dran, J. C. Interactions of U(VI), Nd, and Th(IV) at the calcite-solution interface. *Radiochim. Acta* **1992**, *58–9*, 245.
(8) Geipel, G.; Reich, T.; Brendler, V.; Bernhard, G.; Nitsche, H. Laser and X-ray spectroscopic studies of uranium-calcite interface phenomena. *J. Nucl. Mater.* **1997**, *248*, 408.
(9) Zavarin, M.; Roberts, S. K.; Hakem, N.; Sawvel, A. M.; Kersting, A. B. Eu(III), Sm(III), Np(V), Pu(V), and Pu(IV) sorption to calcite. *Radiochim. Acta* **2005**, *93* (2), 93.
(10) Savenko, A. V. Sorption of UO_2^{2+} on calcium carbonate. *Radiochemistry* **2001**, *43* (2), 193.
(11) Fenter, P.; Geissbuhler, P.; DiMasi, E.; Srajer, G.; Sorensen, L. B.; Sturchio, N. C. Surface speciation of calcite observed in situ by high-resolution X-ray reflectivity. *Geochim. Cosmochim. Acta* **2000**, *64* (7), 1221.
(12) Denecke, M. A.; Bosbach, D.; Dardenne, K.; Lindqvist-Reis, P.; Rothe, J.; Yin, R. Z. Polarization dependent grazing incidence (GI)XAFS measurements of uranyl cation sorption onto mineral surfaces. *Phys. Scr.* **2005**, *T115*, 877.
(13) Elzinga, E. J.; Tait, C. D.; Reeder, R. J.; Rector, K. D.; Donohoe, R. J.; Morris, D. E. Spectroscopic investigation of U(VI) sorption at the calcite-water interface. *Geochim. Cosmochim. Acta* **2004**, *68* (11), 2437.
(14) Rihs, S.; Sturchio, N. C.; Orlandini, K.; Cheng, L. W.; Teng, H.; Fenter, P.; Bedzyk, M. J. Interaction of uranyl with calite in the presence of EDTA. *Environ. Sci. Technol.* **2004**, *38* (19), 5078.
(15) Reeder, R. J.; Nugent, M.; Tait, C. D.; Morris, D. E.; Heald, S. M.; Beck, K. M.; Hess, W. P.; Lanzirotti, A. Coprecipitation of uranium(VI) with calcite: XAFS, micro-XAS, and luminescence characterization. *Geochim. Cosmochim. Acta* **2001**, *65* (20), 3491.
(16) Reeder, R. J.; Nugent, M.; Lamble, G. M.; Tait, C. D.; Morris, D. E. Uranyl incorporation into calcite and aragonite: XAFS and luminescence studies. *Environ. Sci. Technol.* **2000**, *34* (4), 638.
(17) Meece, D. E.; Benninger, L. K. The coprecipitation of Pu and other radionuclides with $CaCO_3$. *Geochim. Cosmochim. Acta* **1993**, *57* (7), 1447.
(18) Kitano, Y.; Oomori, T. The coprecipitation of uranium with calcium carbonate. *J.Oceanogr. Soc. Jpn.* **1971**, *27*, 34–42.
(19) Curti, E. Coprecipitation of radionuclides with calcite: estimation of partition coefficients based on a review of laboratory investigations and geochemical data. *Appl. Geochem.* **1999**, *14* (4), 433.
(20) Reeder, R. J.; Elzinga, E. J.; Tait, C. D.; Rector, K. D.; Donohoe, R. J.; Morris, D. E. Site-specific incorporation of uranyl carbonate species at the calcite surface. *Geochim. Cosmochim. Acta* **2004**, *68* (23), 4799.
(21) Kelly, S. D.; Newville, M. G.; Cheng, L.; Kemner, K. M.; Sutton, S. R.; Fenter, P.; Sturchio, N. C.; Spotl, C. Uranyl incorporation in natural calcite. *Environ. Sci. Technol.* **2003**, *37* (7), 1284.
(22) Kelly, S. D.; Rasbury, E. T.; Chattopadhyay, S.; Kropf, A. J.; Kemner, K. M. Evidence of a stable uranyl site in ancient organic-rich calcite. *Environ. Sci. Technol.* **2006**, *40* (7), 2262.
(23) Henderson, L. M.; Kracek, F. C.; Parsons, C. L.; Moore, R. B.; Lind, S. C.; Schaefer, O. C.; Niermann, J. L.; Scholl, C. E.; Strong, R. K.; Mc Coy, H. N.; Ebler, E.; van Rhyn, A. J.; Doerner, H. A.; Hoskins, W. M.; Germann, F. E. E. Die fraktionierte fällung von barium- und radiumchromaten. *Fresenius J. Anal. Chem.* **1928**, *74* (7), 255.
(24) Wang, Y. F.; Xu, H. F. Prediction of trace metal partitioning between minerals and aqueous solutions: A linear free energy correlation approach. *Geochim. Cosmochim. Acta* **2001**, *65* (10), 1529.
(25) Nielsen, A. E.; Toft, J. M. Electrolyte crystal growth kinetics. *J. Cryst. Growth* **1984**, *67* (2), 278.
(26) Parkhurst, D. L.; Appelo, C. A. J. *User's guide to PhreeqC (Version 2)*; US Geological Survey: Denver, CO, 1999.
(27) Hummel, W.; Berner, U.; Curti, E.; Pearson, F. J.; Thoenen, T. Nagra/PSI chemical thermodynamic data base 01/01. *Radiochim. Acta* **2002**, *90* (9–11), 805.
(28) Rothe, J.; Denecke, M. A.; Dardenne, K.; Fanghanel, T. The INE-beamline for actinide research at ANKA. *Radiochim. Acta* **2006**, *94* (9–11), 691.
(29) Rehr, J. J.; Deleon, J. M.; Zabinsky, S. I.; Albers, R. C. Theoretical X-ray absorption fine-structure sqtandards. *J. Am. Chem. Soc.* **1991**, *113* (14), 5135.
(30) Ressler, T. WinXAS: a program for X-ray absorption spectroscopy data analysis under MS-Windows. *J. Synchrotron Radiat.* **1998**, *5*, 118.
(31) Hennig, C.; Tutschku, J.; Rossberg, A.; Bernhard, G.; Scheinost, A. C. Comparative EXAFS investigation of uranium(VI) and -(IV) aquo chloro complexes in solution using a newly developed spectroelectrochemical cell. *Inorg. Chem.* **2005**, *44* (19), 6655.
(32) Ulrich, K.-U.; Rossberg, A.; Foerstendorf, H.; Zanker, H.; Scheinost, A. C. Molecular characterization of uranium(VI) sorption complexes on iron(III)-rich acid mine water colloids. *Geochim. Cosmochim. Acta* **2006**, *70* (22), 5469.
(33) Tai, C. Y.; Hsu, H. P. Crystal growth kinetics of calcite and its comparison with readily soluble salts. *Powder Technol.* **2001**, *121* (1), 60.
(34) Reddy, M. M.; Nancollas, G. H. Calcite crystal growth inhibition by phosphonates. *Desalination* **1973**, *12* (1), 61.
(35) Wasylenki, L. E.; Dove, P. M.; Wilson, D. S.; De Yoreo, J. J. Nanoscale effects of strontium on calcite growth: An in situ AFM study in the absence of vital effects. *Geochim. Cosmochim. Acta* **2005**, *69* (12), 3017.
(36) Burns, P. C.; Ewing, P. C.; Miller, M. L. Incorporation mechanisms of actinide elements into the structures of U^{6+} phases formed during the oxidation of spent nuclear fuel. *J. Nucl. Mater.* **1997**, *245* (1), 1.
(37) Clark, D. L.; Conradson, S. D.; Ekberg, S. A.; Hess, N. J.; Neu, M. P.; Palmer, P. D.; Runde, W.; Drew Tait, C. EXAFS studies of pentavalent neptunium carbonato complexes. Structural elucidation of the principal constituents of neptunium in groundwater environments. *J. Am. Chem. Soc.* **1996**, *118*, 2089.
(38) Volkov, Y. F.; Tomilin, S. V.; Visyashcheva, G. I.; Kapshukow, I. I. Carbonate compounds of pentavalent actinoids with alkali-metal cations. VI. X-ray structure analysis of $LiNpO_2CO_3$ and $NaNpO_2CO_3$. *Radiokhimiya* **1979**, *21* (5), 668.
(39) Brown, I. D. Bond-valence parameters obtained from a systematic analysis of the inorganic crystal-structure database. *Acta Crystallogr., Sect. B: Struct. Sci.* **1985**, *41*, 244.
(40) Warchtow, R. Datensammlung nach der learnt-profile methode für calcit und vergleich mit der background peak background methode (PBP). *Z. Kristallogr.* **1989**, *186*, 300.
(41) Marques Fernandes, M. Schmidt, M. Stumpf, Th. Walther, C. Bosbach, D. Klenze, R. Fanghänel, T. Site-selective time resolved laser fluorescence spectroscopy of Eu^{3+} doped calcite, *Geochim. Cosmochim. Acta* **2007**, (accepted).

ES071790G